RESEARCH ARTICLE

The mechanical and morphological properties of systemic and pulmonary arteries differ in the Madagascar ground boa, a snake without ventricular pressure separation

Benjamin J. van Soldt[1,*], Tobias Wang[2], Renato Filogonio[3] and Carl Christian Danielsen[4]

ABSTRACT

The walls of the mammalian aorta and pulmonary artery are characterized by diverging morphologies and mechanical properties, which have been correlated with high systemic and low pulmonary blood pressure, as a result of intraventricular pressure separation. However, the relationship between intraventricular pressure separation and diverging aortic and pulmonary artery wall morphologies and mechanical characteristics is not understood. The snake cardiovascular system poses a unique model for the study of this relationship, as representatives both with and without intraventricular pressure separation exist. In this study, we performed uniaxial tensile testing on vessel samples taken from the aortas and pulmonary arteries of the Madagascar ground boa, *Acrantophis madagascariensis*, a species without intraventricular pressure separation. We then compared these morphological and mechanical characteristics with samples from the ball python, *Python regius*, and the yellow anaconda, *Eunectes notaeus* – species with and without intraventricular pressure separation, respectively. Our data suggest that although the aortas and pulmonary arteries of *A. madagascariensis* respond similarly to the same intramural blood pressure, they diverge in morphology, and that this attribute extends to *E. notaeus*. In contrast, *P. regius* aortas and pulmonary arteries diverge both morphologically and in terms of their mechanical properties. Our data indicate that intraventricular pressure separation cannot fully explain diverging aortic and pulmonary artery morphologies. Following the law of Laplace, we propose that pulmonary arteries of small luminal diameter represent a mechanism to protect the fragile pulmonary vasculature by reducing the blood volume that passes through, to which genetic factors may contribute more strongly than physiological parameters.

KEY WORDS: Snake, Vessel wall, Blood pressure, Tension, Biomechanics

INTRODUCTION

Strong yet distensible arterial walls are critical for proper function of the vascular tree in animals. Strength is required to withstand high pressures when blood is ejected from the heart during systole, and distensibility is critical to ensure that the major arteries provide capacitance and pulse-pressure smoothing after each cardiac contraction (Shadwick, 1999). These mechanical properties derive from morphological features of the vessel walls, primarily thickness, elastin and collagen content, and the extent and mode of cross-linking and alignment of the elastin and collagen fibers (Dobrin, 1978; Wagenseil et al., 2009). These properties are established during embryological development in response to hemodynamic forces, such as wall shear stress, that continuously drive vascular remodeling (Jones et al., 2006; Reneman et al., 2006). In mammals, abrupt hemodynamic changes occur after birth, when the pulmonary and systemic circuits become fully separated (Langille, 1996). Intriguingly, reports in various mammals suggest that after birth, major structural changes occur in the aorta wall as compared with the pulmonary artery, the former becoming increasingly thicker-walled and stronger than the latter (Gerrity and Cliff, 1975; Leung et al., 1977). These changes probably reflect necessary adaptations to the considerably higher systemic blood pressure as compared with the pulmonary arterial pressure. However, it remains unclear whether intramural blood pressure indeed provides the causative link to differences in arterial wall morphology.

Intraventricular pressure separation describes the ability of the heart to eject blood into the systemic and pulmonary circulations at different pressures. This ability evolved independently in mammals and archosaurs (birds and crocodiles) through the establishment of a full ventricular septum that divides the ventricle into left (systemic) and right (pulmonary) chambers (Hicks, 1998). In contrast, with the exception of pythons and *Varanus* lizards, non-archosaur sauropsids typically lack a complete ventricular septum, resulting in similar systolic pressures in the systemic and pulmonary arteries (Jensen et al., 2014). Reptiles, therefore, represent an interesting possibility to investigate the relationship between pressure separation and arterial mechanical characteristics.

In previous studies, we analyzed the mechanical characteristics of the major arteries of ball pythons (*Python regius*), which have functional intraventricular pressure separation (Jensen et al., 2010a; van Soldt et al., 2015; Zaar et al., 2007), and the yellow anaconda (*Eunectes notaeus*) that lacks intraventricular pressure separation (Filogonio et al., 2018). These studies revealed that the aortas and pulmonary arteries of *P. regius*, as in mammals, differ in their mechanical properties, while they are more similar in *E. notaeus*. However, the similarity in mechanical properties between the aortas and pulmonary arteries of *E. notaeus* was not mirrored in their morphological features, as might have been expected. Thus, it is possible that, while intraventricular pressure separation has profound effects on the morphology of the great arteries, it may not always play the expected causative role.

In the present study, we therefore investigated the mechanical properties of the aortas and pulmonary arteries of the Madagascar

[1]Gladstone Institute of Cardiovascular Disease, J. David Gladstone Institutes, 1650 Owns Street, San Francisco, CA 94158, USA. [2]Aarhus Institute of Advanced Sciences (AIAS), Aarhus University, 8000 Aarhus C, Denmark. [3]Department of Physiological Sciences, Federal University of São Carlos, São Carlos, SP 13565-905, Brazil. [4]Department of Biomedicine, University of Aarhus, Wilhelm Meyers Allé 3, 8000 Aarhus C, Denmark.

*Author for correspondence (benjamin.vansoldt@gladstone.ucsf.edu)

B.J.v.S., 0000-0002-1670-6193; T.W., 0000-0002-4350-3682; R.F., 0000-0002-5436-7102

Table 1. *Acrantophis madagascariensis* specimens used in this study

n	Mass (g)	Experimental procedures
2	499–655	Blood pressure measurements under anesthesia; mechanical testing; determinations of % dry mass; elastin and collagen determination
4	244–308	Blood pressure measurements while conscious and at rest; mechanical testing; determinations of % dry mass; elastin and collagen determination
3	267–299	Mechanical testing; determinations of % dry mass; elastin and collagen determination

A total of *n*=9 specimens of *Acrantophis madagascariensis* were used in this study, representing a range of body mass. While only *n*=6 snakes were used for blood pressure measurements, all snakes were used for mechanical testing and biochemical determinations.

ground boa (*Acrantophis madagascariensis*) and compared these with those of other species to better understand the relationship between intraventricular pressure separation and the mechanical properties of the great arteries. We first show intraventricular blood pressure data which suggest a lack of pressure separation in the ground boa, and then report our findings on the mechanical characteristics of the pulmonary artery and aorta walls. As in *E. notaeus*, we found that the pulmonary arteries are remarkably resilient to high strains, despite lacking apparent strength, and that this likely relates to their surprisingly small diameter, which may negate the need for increased wall strength. We conclude that differences in morphology and mechanical properties between the aorta and pulmonary arteries may be related to a combination of genetic or developmental factors in addition to pressure separation.

MATERIALS AND METHODS
Snake specimens
Nine captive-bred ground boas, *Acrantophis madagascariensis* (Duméril and Bibron 1844), with a body mass ranging from 244 to 655 g (344±46 g, mean±s.e.m., Table 1) were donated by a zoological garden and kept in accordance with §53 of Danish experimental animal welfare regulations (permit ID 2013-15-2934-

00847). Snakes were fed rodents weekly, but fasted for several weeks prior to euthanasia.

Briefly, snakes were used for blood pressure measurements, histology, mechanical testing and biochemical analysis of vessel walls (Table 1). Prior to euthanasia, intraventricular blood pressure was measured in 6 snakes, of which 4 were conscious and at rest, while the other two were anesthetized. Blood pressure measurements were discounted from two snakes because of the poor quality of the recordings. Following euthanasia, 3–4 vessel rings from 7 unique locations were harvested from all 9 snakes (Fig. 1A) for morphological measurements (Fig. 1B) and tensile testing (Fig. 1A). Following tensile testing to rupture, vessel rings from all 9 snakes were retained for absolute collagen content determination. Excess vessel materials were collected and pooled, to enhance measurement reliability, for determination of collagen and elastin content as a percentage of dry mass (Table 2). Vessel samples were derived from one snake for histology. The experimental procedures are described in detail below.

Blood pressure measurements
Systemic and pulmonary blood pressure was measured in two anesthetized snakes by intraventricular and extracardiac cannulation
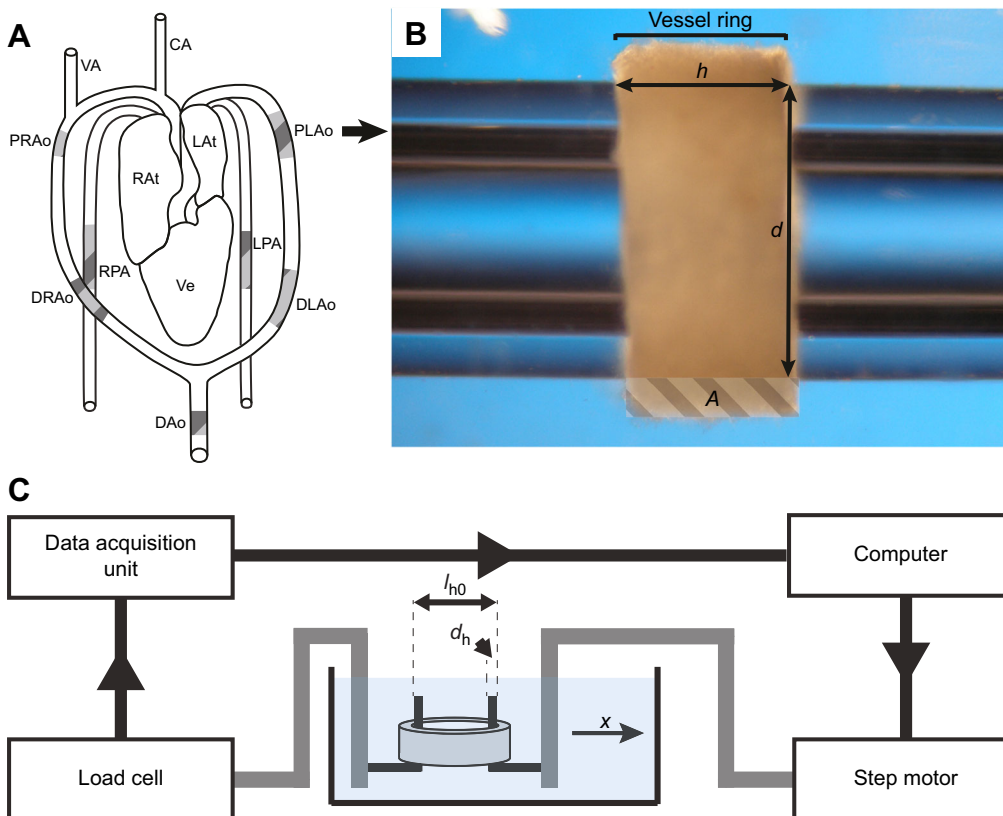
Fig. 1. Methodology overview. (A) Schematic diagram of the *Acrantophis madagascariensis* heart. Striped regions denote the location of sampled vessel sections. VA, vertebral artery; CA, carotid artery; PRAo/PLAo, proximal sections of the right and left aorta; RAt/LAt, right and left atrium; DRAo/DLAo, distal sections of the right and left aorta; RPA/LPA, right and left pulmonary artery; Ve, ventricle; DAo, dorsal aorta. (B) Vessel rings were mounted on a glass rod and photographed in order to measure vessel wall cross-sectional area (wall thickness, *A*), vessel ring height (*h*) and vessel luminal diameter (*d*). (C) Schematic diagram of the mechanical testing experimental setup. Vessel rings were mounted on two orthogonally bent metal hooks with a thickness of d_h (0.55 mm for aortas, 0.35 mm for pulmonary arteries), spaced l_{h0} from each other (1.2 mm for aortas, 0.5 mm for pulmonary arteries). A step motor continuously moved one hook over distance *x*, while a 10 lb (~44.5 N) load cell measured load on the vessel. Adapted from van Soldt et al. (2015). Changes include new acronyms for vessel sections (A), rotation of image and lettering (B), and thicker line art (C).

Table 2. Biochemical determination of vessel ring wall composition in *A. madagascariensis*

Vessel segment	Manner of pooling (snake ID)	n	Elastin content (% dry mass)	Collagen content (% dry mass)
PLAo	1–4, 5–9	2	30.5	21.7
DLAo	1–5, 6–9	2	32.5	19.9
PRAo	1–4, 5–9	2	28.5	21.7
DRAo	1–4, 5–9	2	26.9	21.5
DAo	1–4, 5–9	2	31.0	17.4
LPA	1–9	1	8.9	39.4
RPA	1–9	1	11.1	41.5

Samples from snakes were pooled in a manner that amounted to two batches per aortic segment and one batch per pulmonary artery segment (n). Duplicate determinations were performed per batch. Elastin and collagen content as a percentage of dry mass is given as a mean. PLAo/DLAo, proximal/dorsal sections of the left aorta; PRAo/DRAo, proximal/dorsal sections of the right aorta; DAo, dorsal aorta; LPA/RPA, left and right pulmonary artery.

(vertebral and right pulmonary arteries). Snakes were anesthetized by intramuscular injection of pentobarbital (30 mg kg^{-1}) and anesthesia was confirmed by lack of muscle tone. After subcutaneous application of Xylocain (20 mg ml^{-1}), the cardiac region was exposed through a 10 cm ventral incision. Right aortic and right pulmonary arterial pressure was measured by cannulating the vertebral and right pulmonary artery with PE60 catheters containing heparinized saline (50 IU ml^{-1}). Intraventricular blood pressure was measured in the cavum arteriosum and cavum pulmonale by creating a small incision in the respective ventricular walls and inserting PE90 catheters (see Wang et al., 2003, for details on experimental procedures). To measure systemic blood pressure in four fully recovered snakes, snakes were anesthetized by inhalation of isoflurane, and the dorsal aorta was cannulated in the tail with a PE60 catheter. Pressure measurements were taken 3, 5 and 24 h after recovery from anesthesia. Catheters were connected to Baxter Edward pressure transducers (model PX600, Irvine, CA, USA) placed at heart level of the snakes, and acquired using a Biopac MP100 data acquisition system (Goleta, CA, USA).

Histology
Images of histological sections of vessel segments were obtained from one snake as previously described (van Soldt et al., 2015). Briefly, the segments were fixed in formaldehyde, embedded in paraffin and sectioned (4 μm). The sections were stained with resorcin, Sirius Red F3B and Mayer's hematoxylin. Photographs were taken with an Olympus C-7070 WZ camera (Tokyo, Japan) mounted on a Leica DMRB microscope (Wetzlar, Germany) using both bright field and circular polarization.

Tissue preparation for mechanical testing
All procedures were described previously (van Soldt et al., 2015). After blood pressure measurements were completed, snakes (n=9) were euthanatized (30–50 mg kg^{-1} pentobarbital) and the heart, including great arteries, was excised. Aortic and pulmonary artery segments (~1 cm) were collected from seven locations (left and right pulmonary artery, proximal and distal locations of left and right aorta, and dorsal aorta; Fig. 1A). Vessel segments were cut into 3–4 rings with a nominal length of 1 mm and submerged in 50 mmol l^{-1} Tris-HCl solution (pH 7.4). Wall cross-sectional area (A; Fig. 1B), which corresponds to wall thickness as vessel ring height (h; Fig. 1B) is 1 mm, was measured by mounting the rings on a tapered glass rod at minimal strain, photographed using a Nikon

microscope (Tokyo, Japan; Fig. 1B) with circular polarization filter and analyzed using ImageJ v1.47. A scale was photographed for calibration purposes. Vessel luminal diameter (d; Fig. 1B) was derived from tensile testing data. The rings were then placed at −20°C in 50 mmol l^{-1} Tris-HCl solution (pH 7.4) until mechanical testing. Although no consensus has been reached on the effect of freezing on the mechanical properties of blood vessels (Akyildiz et al., 2014), freezing has not been found to affect mechanical properties significantly across a variety of freeze–thaw procedures (Akyildiz et al., 2014; Chow and Zhang, 2011; Graham et al., 2011; Kesava Reddy, 2004; Stemper et al., 2007).

Mechanical testing
All procedures were described by van Soldt et al. (2015). Briefly, after thawing to room temperature, a vessel ring was placed around two orthogonally bent hooks with a diameter (d_h) of 0.55 mm (aortas) or 0.35 mm (pulmonary arteries) and an initial linear distance between the hooks (l_{h0}) of 1.2 mm and 0.5 mm, respectively (Fig. 1C). One hook was connected to a load cell while a step motor moved the other. Travel distance and load cell readings were acquired continuously. Each ring was subjected to a cycle of five tests with a tension maximum of 0.25 N for the left or right aortas, 0.2 N for the dorsal aorta, and 0.075 N for the pulmonary arteries, because the pulmonary arteries were hypothesized to rupture at lower tension maxima as compared with the aortas. Subsequently, a tension test to rupture was carried out, with maximum travel distance set at the point of vessel rupture (x). Three to four (mean 3.7) rings from each vessel segment were tested. Ruptured rings were collected for hydroxyproline determination (Danielsen and Andreassen, 1988; Woessner, 1976) and absolute collagen content in milligrams was calculated as 7.46×hydroxyproline content (Neuman and Logan, 1950).

Determination of collagen and elastin content
To determine the elastin and collagen fractions relative to dry mass, because of their small size, excess vessel material was pooled into one (pulmonary arteries) or two (aortas) batches. Duplicate determinations were performed per batch. Vessels were defatted with acetone and freeze-dried. Elastin content (percentage of dry mass) was determined after an extraction procedure according to Lansing et al. (1952). Aliquots of the extracts were used for hydroxyproline determination.

Calculation of mechanical properties
Equations have been derived previously (van Soldt et al., 2015). Briefly, we first derived stress (σ) and strain (ε) values as follows:

$$\sigma = \frac{F}{A}, \tag{1}$$

$$\varepsilon = \frac{\Delta l}{l_0}, \tag{2}$$

where F is load, A is cross-sectional area, Δl corresponds to incremental vessel luminal circumference [$l=2(l_{h0}+x-d_h)+(d_h\pi)$], and l_0 corresponds to vessel wall unstrained circumference, recorded as the circumference at a load value of 0.5 mN. Luminal diameter (d; Fig. 1B) was calculated as l_0/π. From recorded load–deformation curves, we derived maximum load (F_{max}) and strain at maximum load (ε_{max}), as well as load–strain and stress–strain curves.

We calculated stiffness (in N) as the slope of the load–strain curve and elastic modulus E (Gibbons and Shadwick, 1989), using stress

and strain, as follows:

$$E = \frac{\Delta\sigma}{\Delta\varepsilon}. \qquad (3)$$

To calculate compliance curves, we first derived relative volume change (V/V_0) from strain values. After simplification:

$$\frac{V}{V_0} = (1 + \varepsilon)^2. \qquad (4)$$

Using load (F) and corresponding strain (ε) values and the law of Laplace as applied to a cylinder, we calculated pressure change (Herman, 2007), giving us:

$$P = \frac{F}{r\,h}, \qquad (5)$$

where h is the nominal height, and the luminal radius (r) is:

$$r = \frac{l_0(1 + \varepsilon)}{2\pi} = \frac{l}{2\pi}, \qquad (6)$$

where $l = l_0(1+\varepsilon)$, so that:

$$P = \frac{F}{r\,h} = \frac{2\pi F}{l_0(1 + \varepsilon)h}. \qquad (7)$$

Stiffness and strain corresponding to pressures of 2, 5 and 10 kPa were then estimated by finding the combination of load and strain fulfilling the equation for P (Eqn 7).

Statistical analysis

Statistical analyses were performed as described previously (van Soldt et al., 2015). Briefly, we ran all statistical analyses in R 4.1.0 (http://www.R-project.org/) running in RStudio v1.4.1717 (https://www.rstudio.com/), using the packages lattice (Sarkar, 2008), lme4 (https://CRAN.R-project.org/package=lme4), car (Fox and Weisberg, 2011) and multcomp (Hothorn et al., 2008). For significance testing of mechanical and morphological properties, we used a mixed model [tested variable as a dependent variable, e.g. F_{max}, and individual animal (Table 1) as a random variable]. A *post hoc* Tukey test was used to identify significant differences between vessel segment pairs ($P<0.05$). Curves were calculated for each vessel section per snake and then combined, per vessel section, into mean curves for presentation in this work. Curve data for proximal and distal segments for both aortas were pooled using described equations (Baker and Nissim, 1963). One-way ANOVA was used for statistical tests on comparisons of morphological parameters between snake species using standard R commands.

RESULTS

Acrantophis madagascariensis lacks intraventricular pressure separation

We confirmed that *A. madagascariensis* lacks intraventricular pressure separation by measuring intraventricular and extracardiac (vertebral and right pulmonary arteries) systemic and pulmonary blood pressure (Fig. 2). Systemic and pulmonary pressure waveforms overlapped entirely for intraventricular pressure measurements, both during systole and diastole. Waveforms for extracardiac measurements overlapped during systole (Fig. 2A). Indeed, systemic and pulmonary systolic pressure were grossly similar at 4.9 and 4.7 kPa, respectively ($n=2$; Fig. 2B and Table 3). To ensure that anesthesia did not have significant effects on blood pressure, we also measured systemic blood pressure in conscious *A. madagascariensis*. Mean arterial blood pressure
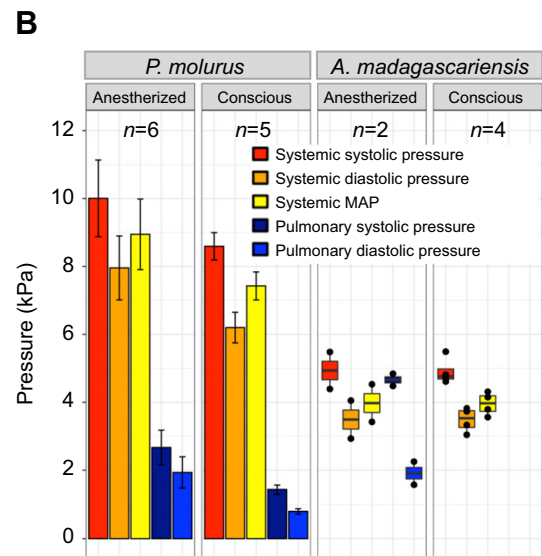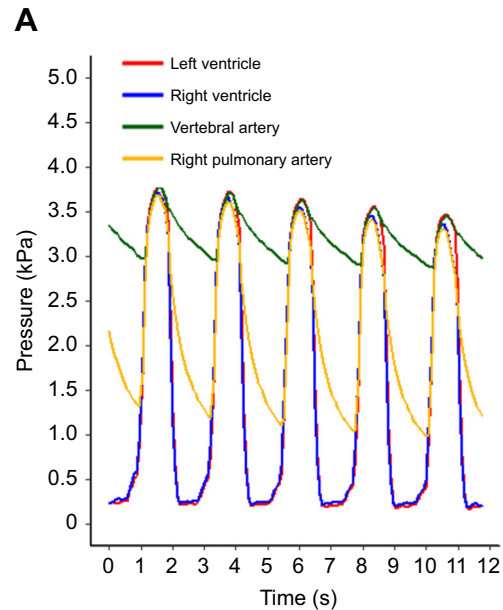

Fig. 2. Systemic and pulmonary blood pressure in *A. madagascariensis* and *Python molurus*. (A) Waveforms showing *A. madagascariensis* left and right intraventricular blood pressure, as well as right aorta (through vertebral artery; see Fig. 1) and right pulmonary artery blood pressure. Based on a single representative specimen. (B) Comparison of systemic and pulmonary systolic, mean arterial pressure (MAP) and diastolic pressure in *P. molurus* and *A. madagascariensis*. Error bars in the *P. molurus* plot indicate s.e.m. (data from Wang et al., 2003). *Acrantophis madagascariensis* box plots display minimum, first quartile, median, third quartile and maximum; points denote individual measurements. Note that *A. madagascariensis* was anesthetized using pentobarbital, and *P. molurus* using halothane.

(MAP) values in anesthetized (4.0 kPa, $n=2$) and conscious (4.0±0.2 kPa, $n=4$) snakes were similar. Thus, these data suggest that *A. madagascariensis* does not have intraventricular pressure separation.

The aortic walls are wider and thicker but more elastic than the pulmonary artery walls

We quantitively determined vessel dimensions (wall thickness, cross-sectional area) by measuring basic morphological parameters

Table 3. Pressure measurements for anesthetized and conscious *A. madagascariensis* and *Python molurus*

	Systemic (kPa)			Pulmonary (kPa)		
	Systolic	Diastolic	MAP	Systolic	Diastolic	MAP
A. madagascariensis						
Anesthetized (*n*=2)	4.94	3.49	3.97	4.66	1.91	2.82
Conscious (*n*=4)	4.9±0.2	3.48±0.18	3.95±0.17	N/A	N/A	N/A
P. molurus						
Anesthetized (*n*=6)	10±1.13	7.98±0.94	8.94±1.04	2.67±0.51	1.93±0.46	2.26±0.48
Conscious (*n*=5)	8.59±0.4	6.2±0.45	7.42±0.41	1.43±0.13	0.8±0.08	1.14±0.11

Systemic and pulmonary blood pressure (systolic, diastolic and mean arterial pressure, MAP) were measured in *A. madagascariensis* (this study) and *P. molurus* (data from Wang et al., 2003) during anesthesia and after recovery (conscious and at rest). Pulmonary pressure was not measured in conscious *A. madagascariensis*. Measurements given as means (anesthetized *A. madagascariensis*) or means±s.e.m. (all others).

of each individual vessel ring using brightfield microscopy (Fig. 1B), and performing biochemical determinations to assess vessel wall composition. The aortic vessels were consistently thicker walled ($P<0.001$, $n=9$; Fig. 3A–M) and of larger diameter than the pulmonary arteries ($P<0.0001$, $n=9$; Fig. 3A–L,N). More specifically, proximal and distal sections of the left (PLAo/DLAo) and right aorta (PRAo/DRAo) were not significantly different in either wall thickness ($P=1$, $P=0.132$; $n=9$; Fig. 3M) or diameter ($P=1$, $P=0.979$; $n=9$; Fig. 3N). However, the left aorta was thicker walled ($P=0.0242$; $n=9$) and wider ($P<0.0001$; $n=9$) than the right aorta (Fig. 3M,N). The dorsal aorta (DAo) was of larger diameter than either the left or right aorta ($P<0.00001$, $n=9$; Fig. 3N). Finally, the right pulmonary artery (RPA) was thicker walled ($P=0.006$, $n=9$) and wider ($P<0.00001$, $n=9$) than the left pulmonary artery (LPA; Fig. 3M,N).

In the vessel wall, the elastin-rich tunica media confers elasticity, while the tunica adventitia – which is composed predominantly of collagen fibers – confers strength. The histology (Fig. 3A–L) illustrates the difference in wall thickness, luminal diameter and tunica adventitia/tunica media ratio between aortic and pulmonary artery specimens. Microscopy using a circular polarization filter indicated that the aortic tunica media was thicker than the tunica adventitia (Fig. 3C,F). In contrast, in the pulmonary artery walls the tunica adventitia was either as thick as, or thicker than, the tunica media (Fig. 3I,L), suggesting that the aortic walls are more elastic than those of the pulmonary arteries. Indeed, determination of elastin and collagen percentage relative to dry mass (Table 2) appeared to suggest that aortic sections had higher elastin content (∼30%), but lower collagen content (∼20%) compared with pulmonary sections (∼9% and ∼40%, respectively), although note that these measurements represent pooled averages (Table 2).

Unit collagen (UC; Fig. 3O) is the collagen content of a vessel ring (in mg) divided by its circumference (in mm). Consistent with the higher collagen percentage of pulmonary artery walls (Table 2), pulmonary artery UC appeared higher than that of the aortas, despite the thinner walls of the pulmonary arteries. This high UC could be explained by the apparently thicker collagen-rich tunica adventitia of the pulmonary arteries (Fig. 3C,F,I,L), and the high collagen content of these arteries. The left aorta had higher UC than the right aorta ($P=0.031$), and the right pulmonary artery had higher UC than the left pulmonary artery ($P<0.001$). Altogether, these data suggest that the aortic walls are more elastic than the pulmonary artery walls.

The aortic walls are stronger and more compliant than the pulmonary artery walls
We next investigated the mechanical properties of the aorta and pulmonary artery walls by subjecting vessel sections to 5 cycles of uniaxial mechanical tension testing, followed by a test to rupture.

Loop curves demonstrated that steady state was reached by the fourth cycle for both aortic and pulmonary artery vessel segments (Fig. 4A). Although load limits in cycle tests were set according to the expected maximal load that the vessel segments could endure without premature rupture (see Materials and Methods), calculation of mechanical hysteresis (viscous damping, loss of elastic energy; loop area divided by area under the loading curve) showed that the pulmonary artery walls were significantly less elastic than those of the aorta ($P<0.0001$, $n=9$; Fig. 4B). Pulmonary arteries also experienced higher load and stress than aortic segments at low strains, and ruptured at significantly lower load and stress values, indicating that the pulmonary artery walls are weaker than the aortic walls ($P<0.001$, $n=9$; Fig. 4C–E). All aortic segments performed similarly. The left and right pulmonary artery segments also performed similarly initially, but at higher strains ($ε>0.4$) the right pulmonary artery displayed steeper load–strain and stress–strain relationships than the left pulmonary artery (Fig. 4C,D). Because left and right aortic distal and proximal sections did not differ in their mechanical properties ($P=0.152$, $P=0.688$, respectively; $n=9$), we pooled data for these sections and treated them as complete left and right aorta hereafter.

The load a vessel wall can endure is linked to gross morphological properties, such as cross-sectional area and collagen content. We therefore normalized maximum load values for these two variables to obtain maximum stress and maximum load/unit collagen, the latter of which may be regarded as a measure of 'collagen quality' (Fig. 5). In both cases, significant relationships between pulmonary artery and aorta sections persisted ($P<0.001$, $n=9$), suggesting that additional morphological factors, besides those investigated here, contribute to the differences in load that these vessels can endure.

Compliance curves calculated from load–strain curves corroborated the relative elasticity of the aortic sections (Fig. 4F). While both the aorta and pulmonary artery walls demonstrated a strong initial relative volume change, these were smaller for the pulmonary arteries (Fig. 4F). Surprisingly, as demonstrated by plotting systolic pressure with the compliance curves, all vessels appeared to operate within the shallow portion of the curve (Fig. 4F), affording them less flexibility in coping with increased blood pressure. Despite these differences in compliance, the elastic modulus, which quantifies the resistance of a vessel wall to deformation, was similar for all tested vessel segments over a broad range of pressure (Fig. 4G), although MAP normalization of pressure indicated that at higher values the elastic modulus of the pulmonary arteries deviated from that of the aortas. Altogether, mechanical tensile testing of aortic and pulmonary artery segments indicated that the pulmonary artery walls were weaker and less distensible than the aortic walls, which may relate to structural features other than those investigated here.
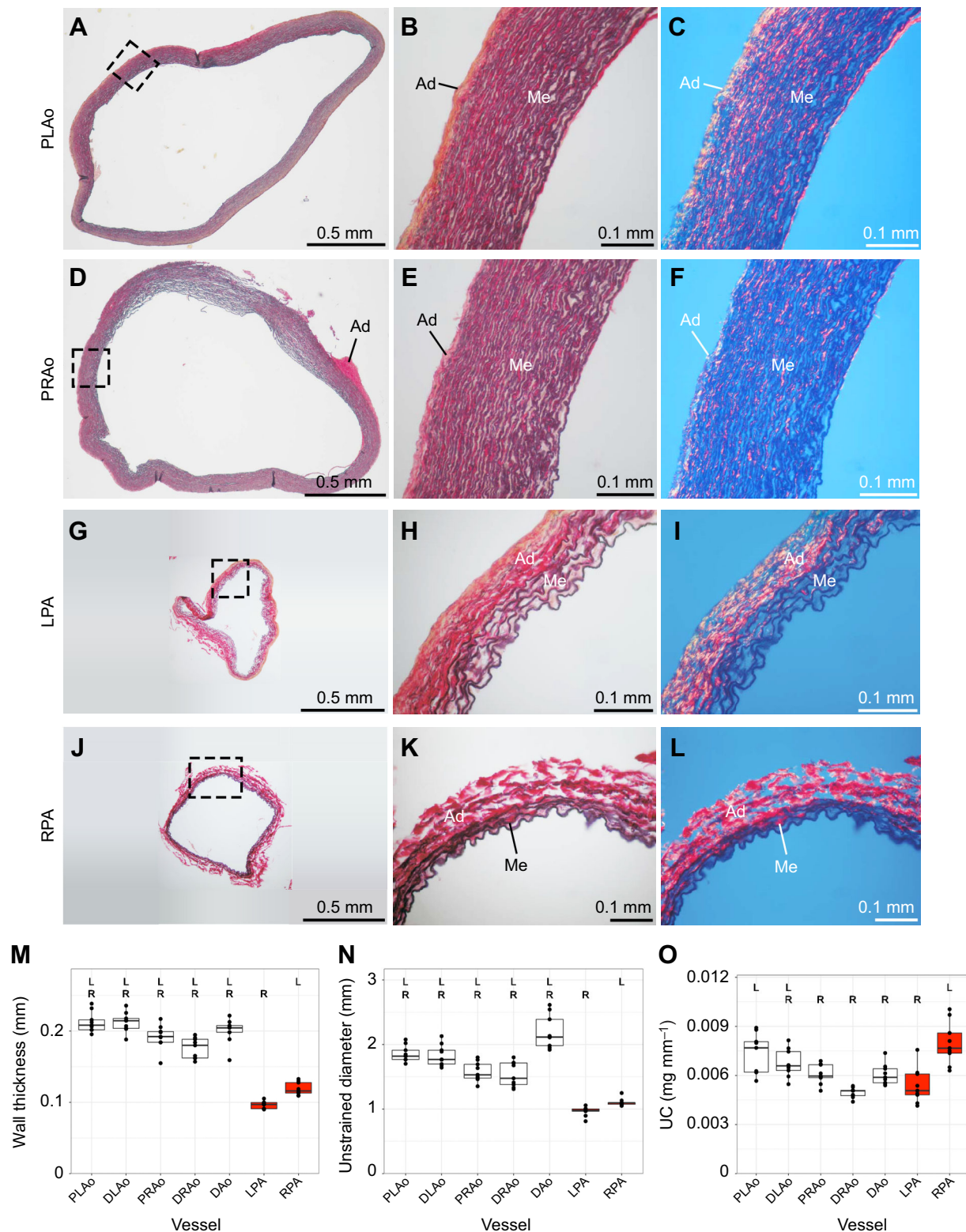
Fig. 3. Histology and quantification of dimensions and collagen content of *A. madagascariensis* aorta and pulmonary artery. (A–L) Brightfield (left and center) and circular polarization (right) images of proximal sections of left (PLAo; A–C) and right aorta (PRAo; D–F), and left (LPA; G–I) and right pulmonary artery (RPA; J–L) of one snake. The aortas are wider and thicker walled than the pulmonary arteries. Note that blank, color-matched borders were added around the vessel section photographs in G and J in order to allow display of LPA and RPA vessel sections at the same magnification as the PLAo and PRAo. Ad, tunica adventitia; Me, tunica media. (M–O) Box plots (minimum, first quartile, median, third quartile and maximum; points denote mean values per snake, *n*=9 snakes, derived from measurements from 3 or 4 vessel rings each) depicting vessel wall thickness (M), unstrained luminal diameter (N) and collagen content normalized by vessel circumference (unit collagen, UC; O). DLAo/DRAo, distal section of the left and right aorta; DAo, dorsal aorta. 'R' and 'L' indicate a significant difference between data for the respective vessel section and the right or left pulmonary artery (*P*<0.05). *P*-values were calculated using a mixed model with *post hoc* Tukey test.
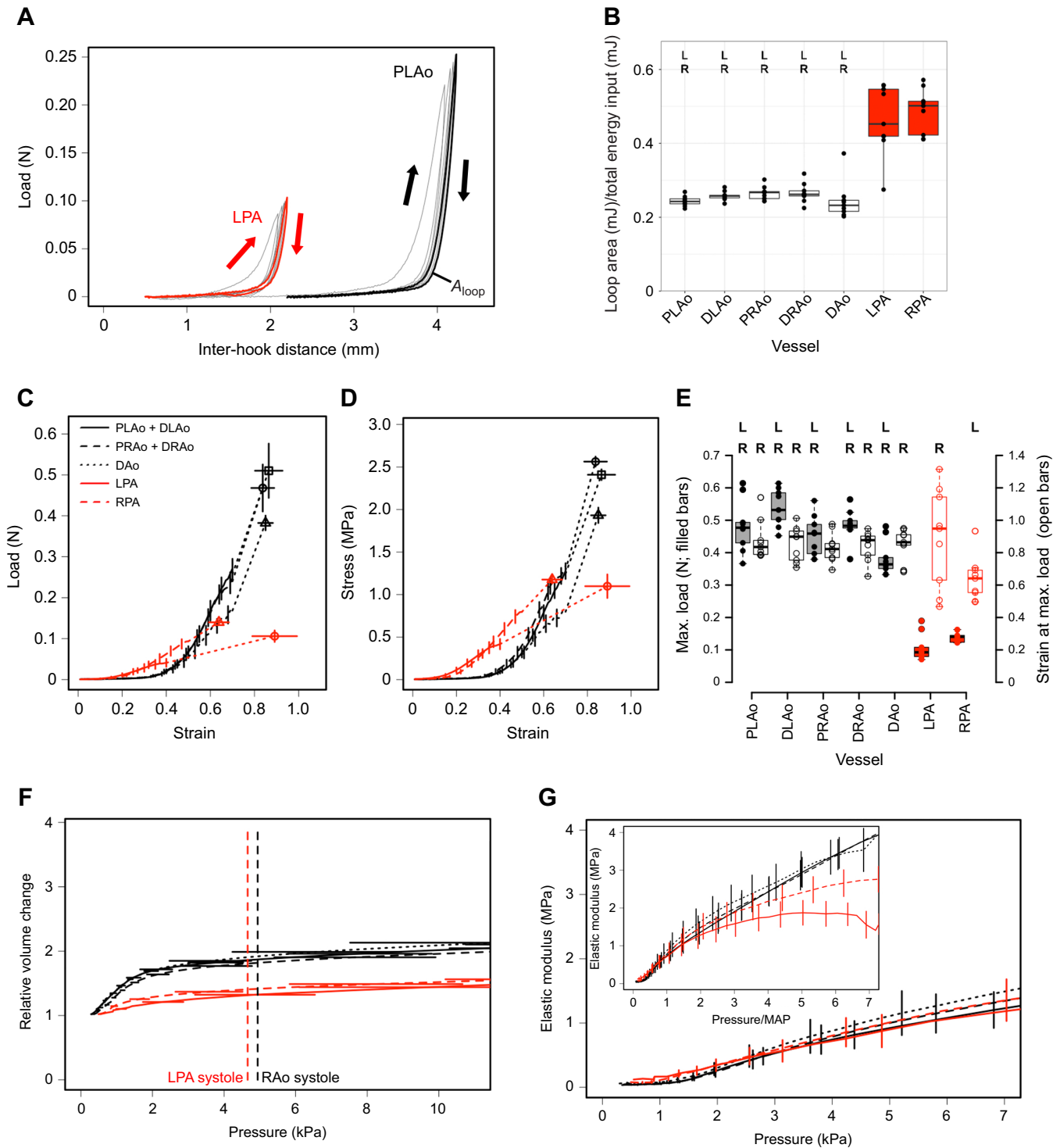
Fig. 4. The pulmonary artery walls of *A. madagascariensis* are weaker and less distensible than the aortic walls. (A) Representative aortic and pulmonary artery loop curves derived from 5-cycle uniaxial mechanical tension testing. Cycles one to four are gray; the fifth cycle is black (proximal segment of left aorta, PLAo) or red (left pulmonary artery, LPA). Up and down arrows denote loading and unloading segments of the cycle graphs, respectively. The area within the loading/unloading curves is termed the 'loop area' (A_{loop}). (B) Box plot (minimum, first quartile, median, third quartile and maximum; points denote mean values per snake, $n=9$ snakes, derived from measurements from 3 or 4 vessel rings each) showing hysteresis (viscous damping), calculated from the fifth tension test cycle (black/red lines in A) by dividing A_{loop} (see A) by the area under the loading curve. 'R' and 'L' indicate a significant difference between data for the respective vessel section and the right or left pulmonary artery ($P<0.05$). P-values were calculated using a mixed model with *post hoc* Tukey test. (C–E) Load–strain (C) and stress–strain curves (D), and (E) box plots showing maximum load (filled bars) and strain at maximum load (open bars). Load–strain and stress–strain curves in C and D are connected by dotted lines to maximum load/strain and stress/strain values (symbols); box plot in E as per B. (F,G) Compliance–pressure (F) and elastic modulus–pressure curves (G) derived from uniaxial mechanical tension testing to rupture. Compliance curves include indications of systolic pulmonary and aortic blood pressure (red and black dashed lines, respectively). The elastic modulus was calculated from differentiated load–strain data divided by vessel wall cross-sectional area and plotted against pressure change (G) or pressure change normalized for mean arterial blood pressure (MAP) values (G inset; 4.94 kPa aortic MAP; 3.49 kPa pulmonary MAP). Left and right aorta curves represent pooled data from respective proximal and distal segments. $n=9$ snakes for all vessel sections.
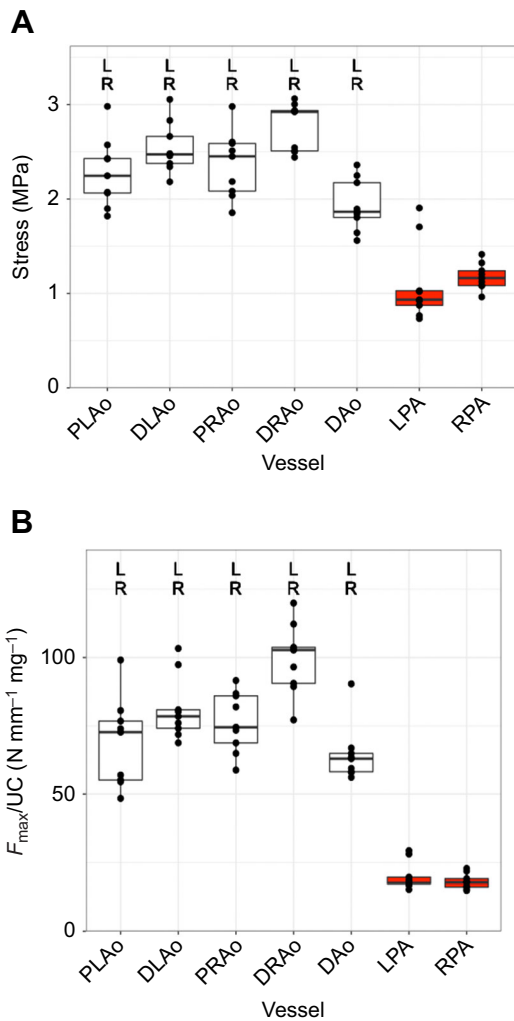
Fig. 5. The pulmonary arteries are structurally weaker than the aortas in *A. madagascariensis*. Box plots (minimum, first quartile, median, third quartile and maximum; points denote mean values per snake, $n=9$, derived from measurements from 3 or 4 vessel rings each) depict normalized values of maximum load (F_{max}) per cross-sectional area (maximum stress, σ_{max}) (A) and per unit collagen (UC; B). 'R' and 'L' indicate a significant difference between data for the respective vessel section and the right or left pulmonary artery ($P<0.05$). P-values were calculated using a mixed model with *post hoc* Tukey test.

Intraventricular pressure separation polarizes aorta and pulmonary artery vessel wall behavior in response to intramural blood pressure

Our data indicate that, despite the lack of intraventricular pressure separation, *A. madagascariensis* pulmonary artery and aorta walls are morphologically different, and this is reflected in the mechanical properties of these vessels. To better understand the role of intraventricular pressure separation in defining aorta and pulmonary artery mechanical characteristics, we assessed comparative vessel mechanical function in the context of cardiovascular physiology of species with (*P. regius*; van Soldt et al., 2015) and without (*A. madagascariensis*) intraventricular pressure separation. We calculated vessel stiffness, modulus and strain at increasing intramural blood pressure of 2, 5 and 10 kPa (Fig. 6), coinciding with systemic and pulmonary systolic pressure of *A. madagascariensis* (both 5 kPa) and *P. regius* (10 and 2.7 kPa, respectively; Fig. 2B). Vessel strain captures

deformation, while vessel stiffness describes resistance against deformation, in a manner where high stiffness correlates with low strain and vice versa. Finally, modulus normalizes stiffness for vessel cross-sectional area, facilitating inter-vessel comparisons.

Our calculations showed that with increasing intramural blood pressure, stiffness (representing absolute resistance to deformation), modulus and strain values significantly increased for all vessels regardless of species (Fig. 6A,B). However, the relative increases in stiffness, modulus and strain from 2 to 5 kPa and 5 to 10 kPa differed between species and between vessels. In *A. madagascariensis*, stiffness increased more steeply in aortic segments (from ∼0.025 to ∼0.06 and ∼0.235, $P<0.0001$; $n=9$, Fig. 6A) compared with pulmonary segments (from ∼0.025 to 0.04 and ∼0.1, $P=0.0249$ and $P<0.001$, respectively; $n=9$; Fig. 6A). Intriguingly, the reverse was true for *P. regius*, where stiffness increased more steeply in the two pulmonary arteries, though at different rates (on average from ∼0.025 to ∼0.15 and ∼0.3, $P<0.0001$; $n=9$, Fig. 6A), compared with the aortas (∼0.025 to ∼0.028 and ∼0.09, $P=0.0042$ and $P<0.001$, respectively; $n=9$, Fig. 6A). However, upon calculation of the modulus, which normalizes stiffness for vessel cross-sectional area, the statistically significant differences between aorta and pulmonary artery vessel walls in *A. madagascariensis* almost entirely disappeared, although relationships from 2 to 5 kPa, and from 5 to 10 kPa, were maintained in a similar fashion to stiffness (Fig. 6B). This suggested that in *A. madagascariensis*, differences in stiffness were explained by differences in vessel wall thickness, whereas in *P. regius*, they might additionally reflect differences in vessel mechanical properties.

In regard to strain, *A. madagascariensis* aortas and pulmonary arteries appeared to operate at significantly different levels of strain but strain increased similarly in response to pressure increases (∼2.5 times from 2 to 10 kPa, $P<0.0001$; $n=9$; Fig. 6C). In *P. regius*, however, the pulmonary arteries operate at higher strains than the aortas at 2 kPa ($P<0.001$, $n=9$; Fig. 6C) and only display, on average, a ∼20% increase in strain at 10 kPa. In addition, the relative increase in strain was comparatively steeper from 2–5 kPa ($P<0.001$, $n=9$; Fig. 6C) than from 5–10 kPa ($P=0.0079$, $n=9$; Fig. 6C). In contrast, the aortas displayed significant, linear increases in strain from 2 to 10 kPa ($P<0.0001$, $n=9$; Fig. 6C). Combined, these data show that in both species, the increase in vessel stiffness is steeper when blood pressure passes above species-specific systolic pressure, resulting in a polarization of vessel mechanical behaviors in *P. regius*, where systemic blood pressure and pulmonary blood pressure are significantly different.

We hypothesized that the observed inter-species differences were associated with differences in vessel morphology. We therefore compared morphological parameters (wall thickness, diameter and unit collagen) of vessel walls between these species (Fig. 6D–F). Intriguingly, while wall thickness did not differ (Fig. 6D), *A. madagascariensis* had significantly narrower pulmonary arteries ($P<0.001$, $n=9$; Fig. 6E) with a higher unit collagen ($P<0.001$, $n=9$; Fig. 6F) than *P. regius*. Intriguingly, these differences were mirrored by *E. notaeus*, highlighting a putative trend between species with and without intraventricular pressure separation.

Thus, *A. madagascariensis* pulmonary arteries are significantly narrower and weaker than aortas, but nevertheless respond similarly to increases in blood pressure. This stands in contrast to *P. regius*, where aortas and pulmonary arteries respond differently to increases in blood pressure.
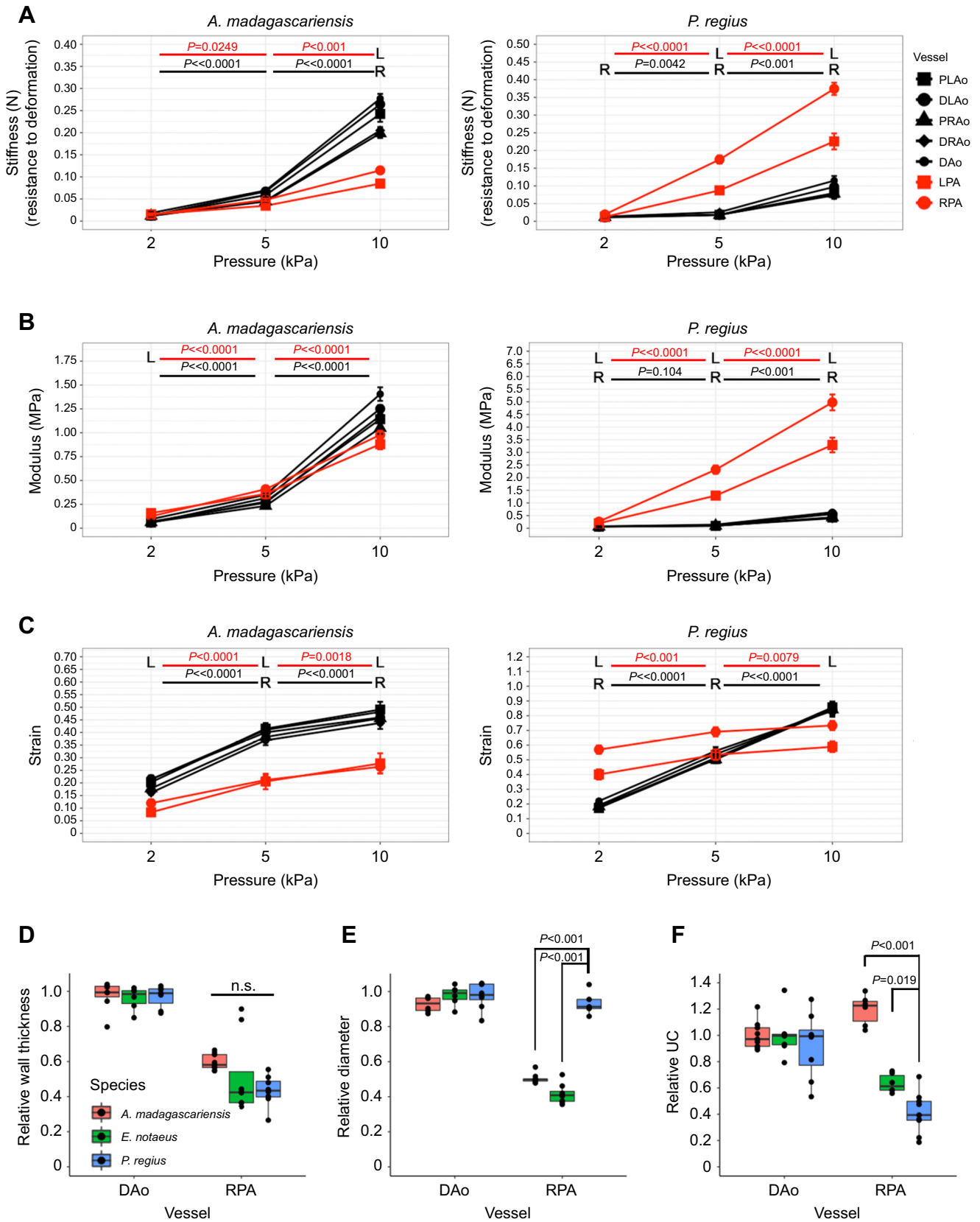
Fig. 6. See next page for legend.

Fig. 6. Species comparisons of functional and morphological variables suggest consistent morphological and operational differences between species with (*Python regius*) and without (*A. madagascariensis*, *Eunectes notaeus*) intraventricular pressure separation. (A–C) Line plots showing change in stiffness (A), modulus (B) and strain (C) of aortic and pulmonary vessels at increasing blood pressure in *A. madagascariensis* (left, *n*=9) and *P. regius* (right, *n*=9). 'R' and 'L' indicate a significant difference between the right or left pulmonary artery and the aortic vessel sections at the corresponding intramural blood pressure, while red and black horizontal bars and *P*-values (see Materials and Methods) correspond to significant differences of stiffness and strain values between the respective intramural blood pressures. n.s., not significant. (D–F) Species comparisons of dorsal aorta (DAo) and right pulmonary artery (RPA) wall thickness (D), luminal diameter (E) and unit collagen (UC; F) normalized for corresponding values of dorsal aorta between *A. madagascariensis* (red, this study; *n*=9), *E. notaeus* (green; Filogonio et al., 2018; *N*=8) and *P. regius* (blue; van Soldt et al., 2015; *n*=9). Box plots display minimum, first quartile, median, third quartile and maximum; points denote mean values per snake, derived from measurements from 3 or 4 vessel rings each. *P*-values in D–F were calculated using a one-way ANOVA.

DISCUSSION

Thoma (1893) was the first to propose that blood circulation impacts blood vessel morphogenesis, describing relationships between blood flow and vessel radius, as well as blood pressure and wall thickness (see Wagenseil and Mecham, 2009). Indeed, the wall of the mammalian aorta is thick and strong in comparison to that of the pulmonary artery, and these differences are associated with high systemic and low pulmonary blood pressure as a result of intraventricular pressure separation postnatally (Gerrity and Cliff, 1975; Leung et al., 1977). Here, we present measurements from *Acrantophis madagascariensis* demonstrating that morphological and mechanical characteristics of the aorta and pulmonary artery can diverge even in the absence of intraventricular pressure separation, corroborated by data from *E. notaeus* (Filogonio et al., 2018).

The absence of intraventricular pressure separation in *A. madagascariensis* is obvious when considering data from *Python molurus* (Fig. 2B; Wang et al., 2003). Here, systemic systolic pressure (10.01±1.13 kPa) is higher than pulmonary systolic pressure (2.67±0.51 kPa). Importantly, *P. molurus* systemic systolic pressure was higher (*P*=0.032) and pulmonary systolic pressure lower (*P*=0.049) than in *A. madagascariensis*.

Despite differences in morphology and mechanical characteristics between *A. madagascariensis* aorta and pulmonary artery walls, these vessels nevertheless responded similarly to increasing wall tension within physiological blood pressure ranges. In contrast, *P. regius* aorta and pulmonary artery responded differently, consistent with the intraventricular pressure separation in this species that polarizes systemic and pulmonary blood pressure. For example, the stiffness and modulus of all *A. madagascariensis* vessels increased more steeply from 5 to 10 kPa than from 2 to 5 kPa, in line with a blood pressure of 5 kPa (Fig. 6A,B). In contrast, *P. regius* pulmonary artery stiffness increased dramatically at pressures over 2 kPa, reflecting the systolic pulmonary blood pressure of 2.7 kPa. This aligns with stiffness/ strain calculations in human and pig, where the pulmonary artery was also stiffer than the aorta at systemic blood pressure (Azadani et al., 2012; Matthews et al., 2010). Thus, the aorta and pulmonary artery are each optimized to handle respective physiological blood pressures, regardless of whether these are equal or divergent.

We were initially surprised that *A. madagascariensis* pulmonary arteries withstood the same blood pressure as the aorta, given their lower strength. However, the law of Laplace intuitively explains that narrow pulmonary arteries do not require strong, thick walls (high cross-sectional area) (Burton, 1965; Shadwick, 1999;

Valentinuzzi and Kohen, 2011). Indeed, the pulmonary arteries of *A. madagascariensis* and *E. notaeus* were narrower than those of *P. regius*, but with similar wall thickness (Fig. 6D,E). Thus, the reduction of pulmonary artery radius may be a mechanism to withstand high pulmonary blood pressure in species that lack intraventricular pressure separation.

While theoretically compelling, the narrow pulmonary arteries of *A. madagascariensis* and *E. notaeus* were surprising, as narrow vessels implicate low blood volume. Studies in sheep demonstrated that abdominal blood flow and vessel diameter decreased concurrently postnatally (Bendeck and Langille, 1992; Bendeck et al., 1994; Langille, 1996; Langille et al., 1990). In rabbit, aorta and pulmonary artery diameter remain similar postnatally while aorta wall thickness increases, likely to accommodate increasing aortic blood pressure (Leung et al., 1977). Likewise, in *P. regius*, we previously found that aorta and pulmonary artery diameter were similar, but the aortic wall was thicker (van Soldt et al., 2015). Thus, one possible explanation for the narrow pulmonary arteries in *A. madagascariensis* and *E. notaeus* includes the capacity for right-to-left cardiac shunts, whereby systemic blood bypasses the lungs for systemic recirculation, potentially decreasing pulmonary blood flow (Hicks, 1998). *Python regius* has limited capacity for such shunts (Jensen and Wang, 2009; Jensen et al., 2010b; Wang et al., 2003), and in mammals, such shunts are impossible because of the physical separation of systemic and pulmonary circuits (Hicks, 1998). Thus, these animals may require a wider pulmonary artery to accommodate the volume of blood flowing through these vessels, instead gaining a thicker aortic vessel wall to accommodate the higher systemic blood pressure. Indeed, in the American alligator, *Alligator mississippiensis*, a species with complete ventricular separation but with an ability to promote right-to-left shunts through the foramen of Panizza, the left pulmonary artery is narrower than the right aorta, corroborating the hypothesis (Filogonio et al., 2021). However, further study is required to ascertain the level of intracardiac shunting in *A. madagascariensis* and *E. notaeus*, and the relationship between the separation of systemic and pulmonary circulation and the diameter of the aorta and pulmonary arteries.

We showed that pulmonary artery unit collagen was markedly higher in *A. madagascariensis* and *E. notaeus* compared with that in *P. regius*. Blood vessel wall structure is fundamentally similar across species, but collagen and elastin content are known to differ to change vessel mechanical properties (Shadwick, 1998, 1999). Wall stiffness is primarily mediated by collagen, suggesting that high unit collagen may complement reduced vessel diameter to strengthen the pulmonary arteries (Dobrin, 1978; Sage and Gray, 1979). Structural features of collagen that were not analyzed here, such as fiber diameter, type, cross-linking and alignment, could further contribute to a role for collagen in strengthening pulmonary artery walls (Ottani et al., 2001). Other components of the extracellular matrix, such as glycosaminoglygans, may also determine several morphological and mechanical characteristics of the arterial wall (Gandley et al., 1997).

Given that our data suggest that intraventricular pressure separation alone may not define gross morphological characteristics of the aorta and pulmonary artery, we suggest that ontogenetic factors may also contribute. The endothelium of the dorsal aorta arises through vasculogenesis from the splanchnic mesoderm (DeSesso, 2017), while that of the pulmonary arteries derives from mesodermal progenitors that originate at the posterior pole of the heart and give rise to a vascular plexus that later connects to the pharyngeal arch arteries (DeRuiter et al., 1993; Peng and Morrisey, 2013; Peng et al., 2013). This apparently divergent

ontogeny may therefore establish diverging transcriptional programs that ultimately shape different vascular morphologies.

In conclusion, we showed that the absence of intraventricular pressure separation in *A. madagascariensis* does not equalize the morphologies and mechanical characteristics of its aorta and pulmonary artery. We propose that, to mitigate a higher wall tension as a consequence of increased pulmonary blood pressure, the pulmonary artery became narrower and the collagen content of its wall increased. However, this may only be possible in species with a capacity for right-to-left cardiac shunts as a mechanism to decrease pulmonary blood flow. Finally, we suggest that ontogenetic differences may be fundamental to the morphological differences between these arteries. Thus, in evolution, compensatory mechanisms to accommodate a range of intramural blood pressures may have followed the law of Laplace in different and sometimes unexpected ways.

Competing interests
The authors declare no competing or financial interests.

Author contributions
Conceptualization: B.J.v.S., T.W.; Methodology: B.J.v.S., T.W., R.F., C.C.D.; Software: C.C.D.; Validation: B.J.v.S., C.C.D.; Formal analysis: B.J.v.S., R.F., C.C.D.; Investigation: B.J.v.S., R.F., C.C.D.; Resources: T.W., C.C.D.; Data curation: B.J.v.S., R.F., C.C.D.; Writing - original draft: B.J.v.S., T.W., R.F., C.C.D.; Writing - review & editing: B.J.v.S., T.W., R.F., C.C.D.; Visualization: B.J.v.S., C.C.D.; Supervision: T.W., C.C.D.; Project administration: B.J.v.S., T.W., C.C.D.; Funding acquisition: B.J.v.S., T.W., R.F.

References
Akyildiz, A. C., Speelman, L. and Gijsen, F. J. H. (2014). Mechanical properties of human atherosclerotic intima tissue. *J. Biomech.* **47**, 773-783. doi:10.1016/j.jbiomech.2014.01.019

Azadani, A. N., Chitsaz, S., Matthews, P. B., Jaussaud, N., Leung, J., Wisneski, A., Ge, L. and Tseng, E. E. (2012). Biomechanical comparison of human pulmonary and aortic roots. *Eur. J. Cardio-Thoracic Surg.* **41**, 1111-1116. doi:10.1093/ejcts/ezr163

Baker, R. W. R. and Nissim, J. A. (1963). Expressions for combining standard errors of two groups and for sequential standard error. *Nature* **198**, 1020. doi:10.1038/1981020a0

Bendeck, M. P. and Langille, B. L. (1992). Changes in blood flow distribution during the perinatal period in fetal sheep and lambs. *Can. J. Physiol. Pharmacol.* **70**, 1576-1582. doi:10.1139/y92-226

Bendeck, M. P., Keeley, F. W. and Langille, B. L. (1994). Perinatal accumulation of arterial wall constituents: relation to hemodynamic changes at birth. *Am. J. Physiol. Circ. Physiol.* **267**, H2268-H2279. doi:10.1152/ajpheart.1994.267.6.H2268

Burton, A. C. (1965). *Physiology and Biophysics of the Circulation.* Chicago: Year Book Medical Publishers.

Chow, M.-J. and Zhang, Y. (2011). Changes in the mechanical and biochemical properties of aortic tissue due to cold storage. *J. Surg. Res.* **171**, 434-442. doi:10.1016/j.jss.2010.04.007

Danielsen, C. C. and Andreassen, T. T. (1988). Mechanical properties of rat tail tendon in relation to proximal-distal sampling position and age. *J. Biomech.* **21**, 207-212. doi:10.1016/0021-9290(88)90171-6

DeRuiter, M. C., Gittenberger-de Groot, A. C., Poelmann, R. E., VanIperen, L. and Mentink, M. M. (1993). Development of the pharyngeal arch system related to the pulmonary and bronchial vessels in the avian embryo. With a concept on systemic- pulmonary collateral artery formation. *Circulation* **87**, 1306-1319. doi:10.1161/01.CIR.87.4.1306

DeSesso, J. M. (2017). Vascular ontogeny within selected thoracoabdominal organs and the limbs. *Reprod. Toxicol.* **70**, 3-20. doi:10.1016/j.reprotox.2016.10.007

Dobrin, P. B. (1978). Mechanical properties of arteries. *Physiol. Rev.* **58**, 397-460. doi:10.1152/physrev.1978.58.2.397

Filogonio, R., Wang, T. and Danielsen, C. C. (2018). Analysis of vascular mechanical properties of the yellow anaconda reveals increased elasticity and distensibility of the pulmonary artery during digestion. *J. Exp. Biol.* **221**, jeb177766. doi:10.1242/jeb.177766

Filogonio, R., Dubansky, B. D., Dubansky, B. H., Wang, T., Elsey, R. M., Leite, C. A. C. and Crossley, D. A. (2021). Arterial wall thickening normalizes arterial wall tension with growth in American alligators, Alligator Mississippiensis. *J. Comp. Physiol. B Biochem. Syst. Environ. Physiol.* **191**, 553-562. doi:10.1007/s00360-021-01353-1

Fox, J. and Weisberg, S. (2011). *An {R} Companion to Applied Regression.* SAGE Publications.

Gandley, R. E., McLaughlin, M. K., Koob, T. J., Little, S. A. and McGuffee, L. J. (1997). Contribution of chondroitindermatan sulfate-containing proteoglycans to the function of rat mesenteric arteries. *Am. J. Physiol. Hear. Circ. Physiol.* **273**, H952-H960. doi:10.1152/ajpheart.1997.273.2.H952

Gerrity, R. G. and Cliff, W. J. (1975). The aortic tunica media of the developing rat. I. Quantitative stereologic and biochemical analysis. *Lab. Invest.* **32**, 585-600.

Gibbons, C. A. and Shadwick, R. E. (1989). Functional similarities in the mechanical design of the aorta in lower vertebrates and mammals. *Experientia* **45**, 1083-1088. doi:10.1007/BF01950164

Graham, H. K., Akhtar, R., Kridiotis, C., Derby, B., Kundu, T., Trafford, A. W. and Sherratt, M. J. (2011). Localised micro-mechanical stiffening in the ageing aorta. *Mech. Ageing Dev.* **132**, 459-467. doi:10.1016/j.mad.2011.07.003

Herman, I. P. (2007). Basic physics of pressure and flow of fluids. In *Physics of the Human Body*, pp. 408-411. New York: Springer.

Hicks, J. W. (1998). Cardiac shunting in reptiles. mechanisms, regulation and physiological functions. In *Biology of the Reptilia* (ed. G. Morphology, C. Gans and A. S. Gaunt), Vol. 19, pp. 425-483. Ithaka, NY: SSAR Press.

Hothorn, T., Bretz, F. and Westfall, P. (2008). Simultaneous inference in general parametric models. *Biom. J.* **50**, 346-363. doi:10.1002/bimj.200810425

Jensen, B. and Wang, T. (2009). Hemodynamic consequences of cardiac malformations in two juvenile ball pythons (python regius). *J. Zoo Wildl. Med.* **40**, 752-756. doi:10.1638/2008-0209.1

Jensen, B., Nielsen, J., Axelsson, M., Pedersen, M., Löfman, C. and Wang, T. (2010a). How the python heart separates pulmonary and systemic blood pressures and blood flows. *J. Exp. Biol.* **213**, 1611-1617. doi:10.1242/jeb.030999

Jensen, B., Nyengaard, J. R., Pedersen, M. and Wang, T. (2010b). Anatomy of the python heart. *Anat. Sci. Int.* **85**, 194-203. doi:10.1007/s12565-010-0079-1

Jensen, B., Moorman, A. F. M. and Wang, T. (2014). Structure and function of the hearts of lizards and snakes. *Biol. Rev.* **89**, 302-336. doi:10.1111/brv.12056

Jones, E. A. V., Le Noble, F. and Eichmann, A. (2006). What determines blood vessel structure? Genetic prespecification vs. hemodynamics. *Physiology* **21**, 388-395. doi:10.1152/physiol.00020.2006

Kesava Reddy, G. (2004). AGE-related cross-linking of collagen is associated with aortic wall matrix stiffness in the pathogenesis of drug-induced diabetes in rats. *Microvasc. Res.* **68**, 132-142. doi:10.1016/j.mvr.2004.04.002

Langille, B. L. (1996). Arterial remodeling: relation to hemodynamics. *Can. J. Physiol. Pharmacol* **74**, 834-841. doi:10.1139/y96-082

Langille, B. L., Brownlee, R. D. and Adamson, S. L. (1990). Perinatal aortic growth in lambs: relation to blood flow changes at birth. *Am. J. Physiol. Hear. Circ. Physiol.* **259**, H1247-H1253. doi:10.1152/ajpheart.1990.259.4.H1247

Lansing, A. I., Rosenthal, T. B., Alex, M. and Dempsey, E. W. (1952). The structure and chemical characterization of elastic fibers as revealed by elastase and by electron microscopy. *Anat. Rec.* **115**, 555-575. doi:10.1002/ar.1091140404

Leung, D. Y., Glagov, S. and Mathews, M. B. (1977). Elastin and collagen accumulation in rabbit ascending aorta and pulmonary trunk during postnatal growth. Correlation of cellular synthetic response with medial tension. *Circ. Res.* **41**, 316-323. doi:10.1161/01.RES.41.3.316

Matthews, P. B., Azadani, A. N., Jhun, C.-S., Ge, L., Guy, T. S., Guccione, J. M. and Tseng, E. E. (2010). Comparison of porcine pulmonary and aortic root material properties. *Ann. Thorac. Surg.* **89**, 1981-1988. doi:10.1016/j.athoracsur.2010.03.002

Neuman, R. E. and Logan, M. A. (1950). The determination of collagen and elastin in tissues. *J. Biol. Chem.* **186**, 549-556. doi:10.1016/S0021-9258(18)56248-7

Ottani, V., Raspanti, M. and Ruggeri, A. (2001). Collagen structure and functional implications. *Micron* **32**, 251-260. doi:10.1016/S0968-4328(00)00042-1

Peng, T. and Morrisey, E. E. (2013). Development of the pulmonary vasculature: current understanding and concepts for the future. *Pulm. Circ.* **3**, 176-178. doi:10.4103/2045-8932.109954

Peng, T., Tian, Y., Boogerd, C. J., Lu, M. M., Kadzik, R. S., Stewart, K. M., Evans, S. M. and Morrisey, E. E. (2013). Coordination of heart and lung co-development by a multipotent cardiopulmonary progenitor. *Nature* **500**, 589-592. doi:10.1038/nature12358

Reneman, R. S., Arts, T. and Hoeks, A. P. G. (2006). Wall shear stress - an important determinant of endothelial cell function and structure - in the arterial system in vivo. *J. Vasc. Res.* **43**, 251-269. doi:10.1159/000091648

Sage, H. and Gray, W. R. (1979). Studies on the evolution of elastin - I phylogenetic distribution. *Comp. Biochem. Physiol. B Biochem. Mol. Biol.* **64**, 313-327. doi:10.1016/0305-0491(79)90277-3

Sarkar, D. (2008). *Lattice: Multivariate Data Visualization with R.* New York: Springer.

Shadwick, R. E. (1998). Elasticity in Arteries: a similar combination and stiff materials creates common mechanical of rubbery and some invertebrates properties in blood vessels of vertebrates. *Am. Sci.* **86**, 535-541. doi:10.1511/1998.43.798

Shadwick, R. E. (1999). Mechanical design in arteries. *J. Exp. Biol.* **202**, 3305-3313. doi:10.1242/jeb.202.23.3305

Stemper, B. D., Yoganandan, N., Stineman, M. R., Gennarelli, T. A., Baisden, J. L. and Pintar, F. A. (2007). Mechanics of fresh, refrigerated, and frozen arterial tissue. *J. Surg. Res.* **139**, 236-242. doi:10.1016/j.jss.2006.09.001

Thoma, R. (1893). *Untersuchungen über die Histogenese und Histomechanikdes Gefässsystems.* Stuttgart: Ferdinand Enke.

Valentinuzzi, M. and Kohen, A. (2011). Laplace's law: what it is about, where it comes from, and how it is often applied in physiology [Retrospectroscope]. *IEEE Pulse* **2**, 74-84. doi:10.1109/MPUL.2011.942054

van Soldt, B. J., Danielsen, C. C. and Wang, T. (2015). The mechanical properties of the systemic and pulmonary arteries of python regius correlate with blood pressures. *J. Morphol.* **276**, 1412-1421. doi:10.1002/jmor.20429

Wagenseil, J. E. and Mecham, R. P. (2009). Vascular extracellular matrix and arterial mechanics. *Physiol. Rev.* **89**, 957-989. doi:10.1152/physrev.00041.2008

Wagenseil, J. E., Ciliberto, C. H., Knutsen, R. H., Levy, M. A., Kovacs, A. and Mecham, R. P. (2009). Reduced vessel elasticity alters cardiovascular structure and function in newborn mice. *Circ. Res.* **104**, 1217-1224. doi:10.1161/CIRCRESAHA.108.192054

Wang, T., Altimiras, J., Klein, W. and Axelsson, M. (2003). Ventricular haemodynamics in Python molurus: separation of pulmonary and systemic pressures. *J. Exp. Biol.* **206**, 4241-4245. doi:10.1242/jeb.00681

Woessner, J. F. (1976). Determination of hydroxyproline in connective tissues. In *The Methodology of Connective Tissue Research* (ed. D. A. Hall), pp. 227-233. Oxford: Joynson-Bruvvers Ltd.

Zaar, M., Overgaard, J., Gesser, H. and Wang, T. (2007). Contractile properties of the functionally divided python heart: two sides of the same matter. *Comp. Biochem. Physiol. A. Mol. Integr. Physiol.* **146**, 163-173. doi:10.1016/j.cbpa.2006.10.015